

## Negative ion photoelectron spectroscopy of $\text{OH}^-(\text{NH}_3)$

Rebecca L. Schwartz, Gustavo E. Davico, Joseph B. Kim, and W. Carl Lineberger<sup>a)</sup>

*JILA, University of Colorado and National Institute of Standards and Technology,  
and Department of Chemistry and Biochemistry, University of Colorado, Boulder, Colorado 80309-0440*

(Received 1 October 1999; accepted 23 December 1999)

The 351 nm photoelectron spectra of  $\text{OH}^-(\text{NH}_3)_n$ ,  $n=1,2$  and the deuterated analogs exhibit two broad peaks. *Ab initio* calculations of the anion and neutral potential-energy surfaces have been carried out using an MP2 (second-order Møller–Plesset)/6-31++G\*\* basis set. The geometries, frequencies, and energetics from these calculations aid in the interpretation of the experimental results. An estimate of the  $\text{OH}(\text{NH}_3)$  electron affinity is  $2.35 \pm 0.07$  eV based on experimental and theoretical results. Calculations of the anion vibrational wave functions indicate that following electron photodetachment, the neutral potential-energy surface is accessed from the reactant entrance channel through the transition state region. © 2000 American Institute of Physics.  
[S0021-9606(00)00711-X]

### I. INTRODUCTION

The  $\text{OH} + \text{NH}_3 \rightarrow \text{NH}_2 + \text{H}_2\text{O}$  reaction has been studied both experimentally<sup>1–4</sup> and theoretically.<sup>5–7</sup> This reaction is of great interest because it is the key step in the oxidation of  $\text{NH}_3$  in the atmosphere. It is also an important reaction in the combustion of fossil fuels.

Kinetics experiments have determined the rate constant for this reaction using several different techniques and over a wide range of temperatures.<sup>1–4</sup> The most recent study by Y.-P. Lee and co-workers<sup>4</sup> reported the rate constant to be  $1.18\text{--}4.12 \times 10^{-13} \text{ cm}^3 \text{ molecule}^{-1} \text{ s}^{-1}$  over the temperature range of 273–433 K. Earlier studies by Silver and Kolb<sup>2</sup> extended the temperature range to 1075 K, yielding a rate constant of  $1.93 \times 10^{-12} \text{ cm}^3 \text{ molecule}^{-1} \text{ s}^{-1}$ .

Early *ab initio* studies by Leroy *et al.* utilized the Hartree–Fock method and the 6-31G basis set to study the  $\text{OH} + \text{NH}_3 \rightarrow \text{NH}_2 + \text{H}_2\text{O}$  reaction.<sup>8</sup> More recently, Møller–Plesset perturbation computations have focussed on characterizing the reaction along the reaction coordinate.<sup>5–7,9</sup> Lluh and co-workers<sup>5</sup> have performed high level *ab initio* calculations on both the forward and backward reactions, focusing on the barrier heights and the reaction mechanism. Subsequent calculations by Espinosa–Garcia and co-workers were aimed at determining the geometries and energetics of the intermediate complexes involved in the reaction.<sup>6</sup> The transition state (TS) geometry was determined and an intrinsic reaction coordinate (IRC) was constructed to connect the TS with the minima corresponding to the reactant and product complexes,  $\text{OH}(\text{NH}_3)$  and  $\text{NH}_2(\text{H}_2\text{O})$ , respectively. Reaction-path dynamics calculations have looked at details along the reaction pathway at a higher level, including geometries, relative stabilities of the complexes and the barrier height.<sup>9</sup> Lastly, quantum scattering calculations have been performed on the  $\text{OH} + \text{NH}_3$  reaction yielding a potential-energy surface and information on the reaction products and rate constants.<sup>10</sup>

The  $\text{OH} + \text{NH}_3 \rightarrow \text{NH}_2 + \text{H}_2\text{O}$  reaction is also interesting to study because it is an example of a hydrogen abstraction reaction. Anion photoelectron spectroscopy has been implemented to study other hydrogen abstraction reactions for many years. Neumark and co-workers have focussed their attention on characterizing highly reactive species via negative ion photoelectron spectroscopy.<sup>11–13</sup> Reactions such as  $\text{F} + \text{H}_2$ ,  $\text{I} + \text{HI}$ , and  $\text{Br} + \text{HI}$  have been studied in this way. In all cases, the negative ion of the complex is formed and the neutral potential-energy surface is probed in the region of the transition state. Another prototypical example<sup>14</sup> of “transition state” spectroscopy is the characterization of the  $\text{OH} + \text{H}_2 \rightarrow \text{H}_2\text{O} + \text{H}$  reaction coordinate via the detachment of an electron from  $\text{H}_3\text{O}^-$ . In this case, vibrational excitation of the anion provided access to both reactant and product channels. The transition state of the neutral reaction, however, is not always probed via photodetachment as seen in experiments on  $\text{OH}^-(\text{N}_2\text{O})$ ,  $\text{H}^-(\text{NH}_3)$ , and  $\text{NH}_2^-(\text{NH}_3)$ .<sup>15–17</sup>

In this paper, the neutral potential-energy surface of the  $\text{OH} + \text{NH}_3 \rightarrow \text{NH}_2 + \text{H}_2\text{O}$  reaction is probed via photoelectron spectroscopy of the  $\text{OH}^-(\text{NH}_3)$  complex. Also presented in this paper are results of *ab initio* calculations performed on both the anion and neutral potential-energy surfaces in order to aid in the interpretation of the experimental spectrum. Section II contains details of the experimental and theoretical procedures. Section III describes the results of the experiments and calculations while Sec. IV includes an analysis of these results and comparisons to other relevant experimental and theoretical works. Finally, the conclusions are found in Sec. V.

### II. TECHNIQUES

#### A. Experiment

The details of the negative ion photoelectron spectrometer have been described previously, therefore, only a brief discussion will be provided here.<sup>18</sup> The  $\text{OH}^-(\text{NH}_3)_n$  ( $n=0\text{--}2$ ) anion clusters are produced in a flowing afterglow ion source by reacting  $\text{O}^-$  with  $\text{NH}_3$  in the presence of he-

<sup>a)</sup>Electronic mail: wcl@jila.colorado.edu

lium buffer gas. The O<sup>-</sup> ions are produced by flowing O<sub>2</sub> seeded in helium through a microwave discharge. The NH<sub>3</sub> is introduced downstream through an inlet in order to produce the OH<sup>-</sup> ions and the OH<sup>-</sup>(NH<sub>3</sub>) clusters. The fully deuterated clusters, OD<sup>-</sup>(ND<sub>3</sub>), were studied using ND<sub>3</sub>. The position of the inlet and the flow rates of the gases are modified to optimize the production of the clusters. Once the ions are formed they are accelerated to 735 eV, mass selected, and decelerated to 38 eV before interacting with a fixed frequency, continuous wave Ar ion laser beam positioned orthogonal to the ion beam axis. The 351 nm (3.531 19 eV) line of the Ar ion laser is coupled into a build-up cavity which also serves as the interaction chamber. The photodetached electrons are collected and energy analyzed orthogonal to both the ion and laser beam axes. The typical ion current of the OH<sup>-</sup>(NH<sub>3</sub>) clusters is 100–200 pA at room temperature (300 K). Experiments also were performed under liquid nitrogen cooled conditions. Liquid nitrogen is passed through a metal sleeve that surrounds the flow tube, lowering the vibrational temperature of the anions to ~200 K.

The photoelectron spectra are collected as the number of detached electrons versus the electron kinetic energy (eKE). The spectra presented in this paper also are plotted as a function of electron binding energy (eBE), where  $eBE = h\nu - eKE$ . The polarization of the laser beam can be rotated relative to the direction of the electron collection axis by rotating a wave plate that is positioned in the laser beam path before it enters the interaction chamber. The dependence of the features in the photoelectron spectrum on the polarization of the laser beam provides information on the orbitals and electronic states involved in the photodetachment process. All spectra presented in this paper were recorded at  $\theta = 54.7^\circ$ , the ‘‘magic angle,’’ where  $\theta$  is the angle between the laser polarization and the direction of electron collection. Spectra were also recorded at  $\theta = 0^\circ$  (parallel) and  $90^\circ$  (perpendicular) in order to determine the anisotropy parameter,  $\beta$ .<sup>19</sup>

$$\beta = \frac{I_0 - I_{90}}{(1/2)I_0 + I_{90}}, \quad (1)$$

where  $I_0$  is the intensity of a peak at a specific energy in the  $\theta = 0^\circ$  spectrum and  $I_{90}$  is the intensity of the same peak in the  $\theta = 90^\circ$  spectrum.

## B. Theory

*Ab initio* calculations of the anion and neutral surfaces were performed using the GAUSSIAN 94 suite of programs.<sup>20</sup> Geometry optimizations and frequency calculations were conducted using second-order Møller–Plesset perturbation theory including all electrons (MP2 FULL) and the 6-31++G\*\* basis set. The geometry calculations identified the stationary points on the surfaces and optimized their structures. The frequency calculations confirmed that each stationary point is indeed a minimum or a transition state and aided in the assignment of the peaks in the photoelectron spectra. Single point energy calculations at the stationary points were performed using fourth-order Møller–Plesset

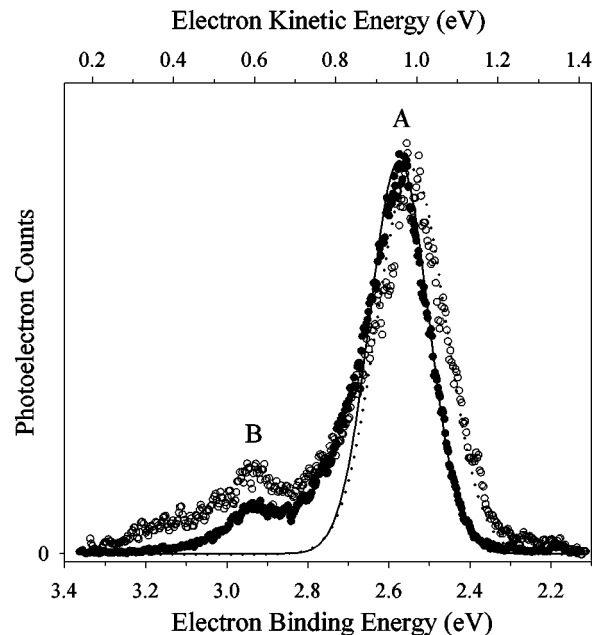


FIG. 1. The 351 nm negative ion photoelectron spectra of OH<sup>-</sup>(NH<sub>3</sub>) recorded at 300 K (○) and 200 K (●). Gaussian functions are used to fit the origin peak, A, to determine the vertical detachment energy and the full width at half maximum (FWHM). The dotted line is the fit to the 300 K spectrum and the solid line is the fit to the 200 K spectrum. The FWHM is 200 meV at 300 K and 170 meV at 200 K. Peak B corresponds to a vibrationally excited transition.

perturbation theory (MP4) and the same basis set. An intrinsic reaction coordinate (IRC) was calculated to map out the reaction coordinate on the neutral surface. The calculation starts at the transition state structure and proceeds toward both reactants and products. Finally, the vibrational wave functions on the anion surface were calculated in order to determine the region of the neutral surface that is accessed upon the photodetachment of an electron from the anion.

## III. RESULTS

### A. Experiment

The photoelectron spectra of OH<sup>-</sup>(NH<sub>3</sub>) recorded at room temperature (300 K) and under liquid nitrogen cooled conditions (200 K) are displayed in Fig. 1 with open and filled circles, respectively. Both spectra contain a main peak, A, and a smaller peak, B, which appears to higher electron binding energy. Since there is no vibrational structure on either of these peaks, it is difficult to make a direct measurement of the adiabatic electron affinity (EA). A determination of this quantity can be made using the results from experiments and calculations, as discussed in Sec. IV B. The vertical detachment energy (VDE), the energy at which the neutral complex has the same geometry as the equilibrium geometry of the anion, can be directly measured and is reported. The VDE and full width at half maximum (FWHM) for each peak were determined by fitting the features to a Gaussian function, shown with the spectra in Fig. 1. The VDEs for peaks A and B at 300 K are  $2.54 \pm 0.015$  and  $2.89 \pm 0.015$  eV, respectively. As seen in Fig. 1, the main difference between the spectrum taken at 300 K and that

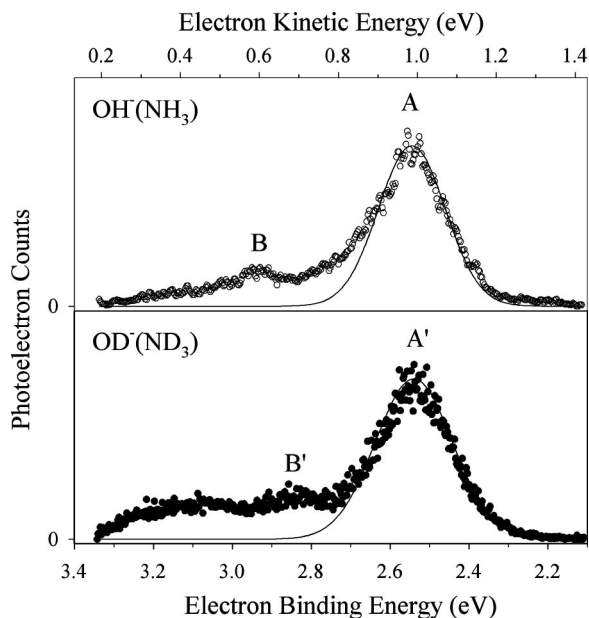


FIG. 2. The 351 nm negative ion photoelectron spectra of  $\text{OH}^-(\text{NH}_3)$  and  $\text{OD}^-(\text{ND}_3)$  recorded at room temperature, 300 K. The solid line in both spectra represent the Gaussians used to fit the peaks in order to extract the peak position and full width at half maximum. The origin peaks,  $A$  and  $A'$ , are at the same electron binding energy,  $2.54 \pm 0.015$  eV. Peak  $B'$  is shifted to lower energy than peak  $B$  by  $\sim 0.06$  eV ( $485$   $\text{cm}^{-1}$ ).

taken at 200 K is that upon cooling the FWHM of peak  $A$  decreases. At 300 K, the FWHM is 200 meV compared to 170 meV at 200 K. This difference is attributed to hot band transitions that appear at low electron binding energy in the room temperature spectrum and are quenched upon cooling. In addition, there is a small shift in the VDE of both peaks,  $A$  and  $B$ , upon cooling the ions, however, the energy difference between the peaks remains equivalent,  $0.35 \pm 0.03$  eV ( $2825$   $\text{cm}^{-1}$ ).

The same experiment was performed on the fully deuterated complex,  $\text{OD}^-(\text{ND}_3)$ , to aid in the assignment of the photoelectron spectrum. The spectrum was recorded at room temperature and is similar to that of  $\text{OH}^-(\text{NH}_3)$  as displayed in Fig. 2. Peaks labeled  $A'$  and  $B'$  correspond to those marked  $A$  and  $B$  in the  $\text{OH}^-(\text{NH}_3)$  spectrum. There is an additional peak at high electron binding energy that arises from  $\text{OD}^-(\text{D}_2\text{O})$ , which has the same mass as  $\text{OD}^-(\text{ND}_3)$ . Peaks  $A'$  and  $B'$  are at  $2.54 \pm 0.015$  and  $2.83 \pm 0.015$  eV and have FWHM of 210 and 200 meV, respectively. The assignments of these peaks are discussed in Sec. IV A.

The 200 K photoelectron spectrum of  $\text{OH}^-(\text{NH}_3)_2$  was also recorded. It is displayed in Fig. 3 along with the  $\text{OH}^-(\text{NH}_3)$  and  $\text{OH}^-$  spectra. The same origin peak is observed, labeled  $A''$ , at an electron binding energy of  $3.05 \pm 0.015$  eV. The breadth of this peak has increased to 245 meV as compared to the 170 meV measured in the  $n=1$  spectrum. A feature corresponding to peak  $B$  is not observed in the  $n=2$  spectrum. This peak could lie at an energy that is higher than the  $3.531$  eV available from the laser or it could be obscured by the breadth of peak  $A''$ . Table I consists of a list of the VDEs and FWHM for the features in the

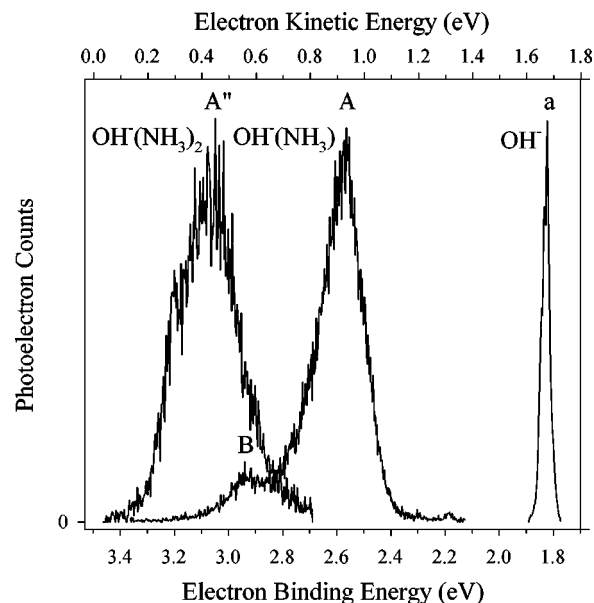


FIG. 3. The 351 nm negative ion photoelectron spectra of  $\text{OH}^-(\text{NH}_3)_n$ ,  $n=0-2$  recorded at 200 K. The origin peaks are labeled  $a$ ,  $A$ , and  $A''$  for  $n=0, 1$ , and  $2$ , respectively. The origin shifts to higher electron binding energy and the full width at half maximum (FWHM) increases upon solvation of  $\text{OH}^-$  by  $\text{NH}_3$ . The increase in the FWHM is attributed to unresolved low-frequency van der Waals vibrations.

$\text{OH}^-(\text{NH}_3)$ ,  $\text{OD}^-(\text{ND}_3)$ , and  $\text{OH}^-(\text{NH}_3)_2$  photoelectron spectra.

The anisotropy parameter,  $\beta$ , for peaks  $A$  and  $B$  in the  $\text{OH}^-(\text{NH}_3)$  spectrum was determined using data from spectra recorded at  $\theta=0^\circ$  and  $90^\circ$ . The value of  $\beta$  was the same for both peaks,  $-0.8$ , which corresponds to preferential electron detachment perpendicular to the laser polarization, suggesting that the electron originates from a  $p$ -type orbital. Since both peaks have the same  $\beta$ , it can be concluded that the same electronic state contributes to all transitions observed in the photoelectron spectrum.

TABLE I. Vertical detachment energies (VDE) and full widths at half maximum (FWHM) for the primary peaks in the  $\text{OH}^-(\text{NH}_3)$ ,  $\text{OD}^-(\text{ND}_3)$ , and  $\text{OH}^-(\text{NH}_3)_2$  photoelectron spectra. Both parameters were determined by fitting the peaks to Gaussian functions. Error on the VDEs is 0.015 eV.

| Peak                                  | VDE (eV) | FWHM (meV) | Relative energy ( $\text{cm}^{-1}$ ) |
|---------------------------------------|----------|------------|--------------------------------------|
| $\text{OH}^-(\text{NH}_3)$ at 300 K   |          |            |                                      |
| $A$                                   | 2.54     | 200        | 0                                    |
| $B$                                   | 2.89     | 190        | 2825                                 |
| $\text{OH}^-(\text{NH}_3)$ at 200 K   |          |            |                                      |
| $A$                                   | 2.58     | 170        | 0                                    |
| $B$                                   | 2.93     | 150        | 2825                                 |
| $\text{OD}^-(\text{ND}_3)$ at 300 K   |          |            |                                      |
| $A'$                                  | 2.54     | 210        | 0                                    |
| $B'$                                  | 2.83     | 200        | 2340                                 |
| $\text{OH}^-(\text{NH}_3)_2$ at 200 K |          |            |                                      |
| $A''$                                 | 3.05     | 245        |                                      |

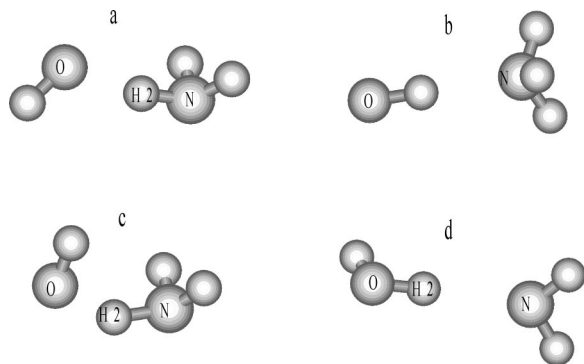


FIG. 4. Geometries of the stationary points along the anion and neutral surfaces found by *ab initio* calculations. There is one stable minimum (a) for the anion corresponding to OH<sup>-</sup>(NH<sub>3</sub>), which is of C<sub>s</sub> symmetry. Structures (b), (c), and (d) are the neutral reactant OH(NH<sub>3</sub>), transition state, and product H<sub>2</sub>O(NH<sub>2</sub>) complexes, respectively. Structures (b) and (c) are of C<sub>1</sub> symmetry and (d) is C<sub>s</sub>. All unlabeled atoms are hydrogen atoms.

## B. Computations

### 1. Anion potential-energy surface

*Ab initio* calculations at the MP2(FULL)/6-31++G\*\* level were performed to search for stationary points along the anion surface. Only one minimum was found corresponding to the reactant complex, OH<sup>-</sup>(NH<sub>3</sub>), located in the entrance channel to the OH<sup>-</sup>+NH<sub>3</sub>→H<sub>2</sub>O+NH<sub>2</sub><sup>-</sup> reaction. No minimum was found for the NH<sub>2</sub><sup>-</sup>(H<sub>2</sub>O) product complex. The geometry of the reactant cluster is shown in Fig. 4(a); it is of C<sub>s</sub> symmetry. In addition to the geometry optimization, vibrational frequencies also were calculated at this stationary point; confirming that this geometry is a minimum on the potential-energy surface.

The anion surface was scanned along the N–H2 bond distance to map out the topology of the surface along this coordinate. H2 is the hydrogen atom that is exchanged upon reaction (see Fig. 4). All other degrees of freedom were optimized at each N–H2 distance. The potential becomes flatter at large N–H2 bond distances before reaching the separated products, NH<sub>2</sub><sup>-</sup>+H<sub>2</sub>O, showing no evidence of an NH<sub>2</sub><sup>-</sup>(H<sub>2</sub>O) minimum. As a result of these calculations, it has been assumed that all of the anion clusters that are formed in the flow tube are best described as OH<sup>-</sup>(NH<sub>3</sub>).

The surface was also mapped out by scanning both the O–H2 and N–O distances ( $r_{OH}$  and  $r_{NO}$ , respectively) while keeping all other parameters constant at the OH<sup>-</sup>(NH<sub>3</sub>) equilibrium geometry values. Values of  $r_{OH}$  were scanned between 0.8 and 2.5 Å and  $r_{NO}$  between 2 and 4 Å in increments of 0.1 Å. The energy was calculated for each point at specific values of  $r_{OH}$  and  $r_{NO}$  and a potential-energy surface was generated. In order to characterize the region near the minimum better, a more detailed scan of the potential energy surface was calculated at intervals of 0.025 Å. The anion potential energy surface is shown in Fig. 5.

### 2. Anion vibrational wave functions

Anion vibrational wave functions have been calculated to identify the overlap between the anion and neutral potentials. Cuts along the long and short diagonals (through the

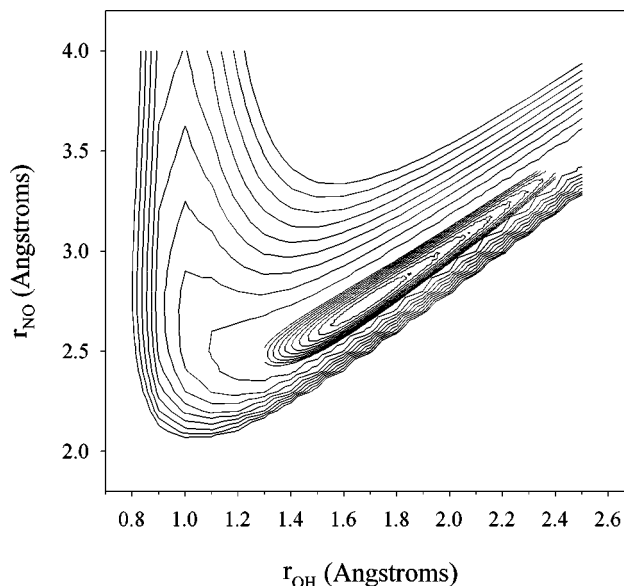


FIG. 5. Contour plot of the anion potential-energy surface. Contours are in increments of 0.2 eV starting at 0.4 eV. Also displayed is a contour plot showing details in the region around the minimum of the potential-energy surface at contour intervals of 0.02 eV with the first contour at 0.02 eV.

minimum) of the potential-energy surface reveal the shape of the potential near the bottom of the well. Although there is evidence of anharmonicity, assuming a harmonic oscillator is a good approximation for vibrational levels lying low in the potential. By fitting the surfaces, frequencies and force constants have been obtained. The frequency along the long diagonal is 230 cm<sup>-1</sup>, approximately a factor of 5 smaller than that calculated in the other direction. The force constants have been used to calculate the probability wave functions  $\Psi_{00}^2$  and  $\Psi_{10}^2$  using the equations for harmonic oscillator wave functions where for  $\Psi_{xy}$ ,  $x$  is the quanta of vibration in O–H2 and  $y$  is the quanta if vibration in N–O.<sup>21</sup> Given the values of the frequencies and the temperature of the experiment (200 K), only the  $\Psi_{00}$  and  $\Psi_{10}$  wave functions have been calculated.

### 3. Neutral

*Ab initio* calculations of the neutral surface at the MP2(FULL)/6-31++G\*\* level have found three stationary points. Both the reactant OH(NH<sub>3</sub>) and product NH<sub>2</sub>(H<sub>2</sub>O) clusters are found to be stable minima relative to their respective asymptotes, even when taking into consideration their zero-point energies. Additionally, the transition state structure has been identified. All of these structures are shown in Figs. 4(b)–4(d) IRC calculations confirm that the TS and product complex [Figs. 4(c) and 4(d)] are connected along the reaction coordinate; however, the pathway from the TS towards the reactants was more difficult to map out. There is a flat region in the potential-energy surface that corresponds to the OH internal rotation within the complex. As illustrated in Figs. 4(b) and 4(c) the OH must undergo a large rotation in order to proceed from the reactant complex geometry to that of the transition state.

The reactant complex, OH(NH<sub>3</sub>), on the neutral surface is very close to C<sub>3v</sub> symmetry with the H atom of the OH

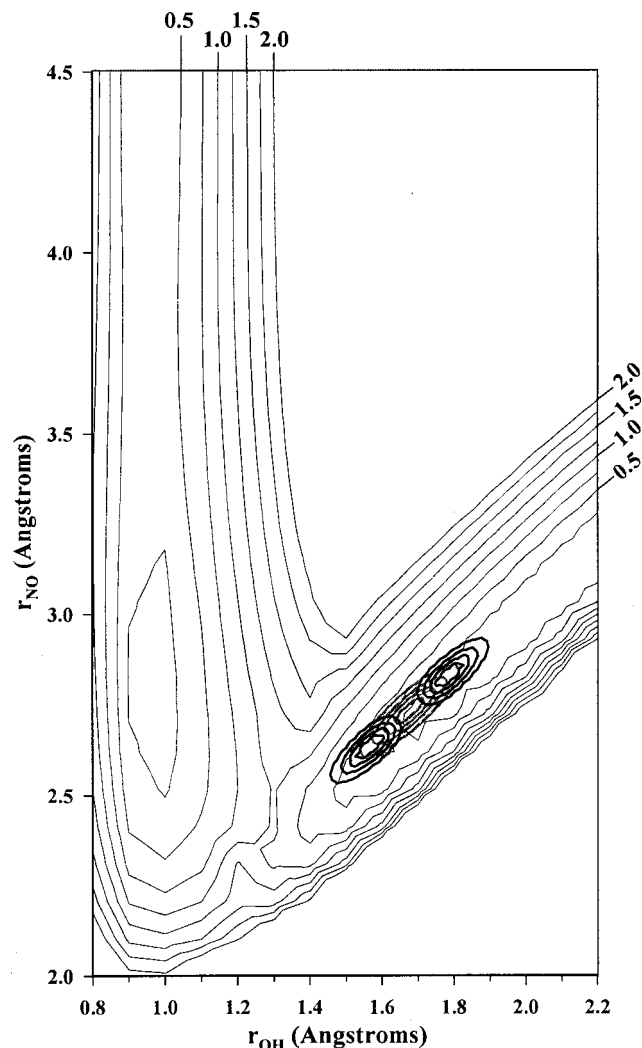


FIG. 6. Contour plot of the neutral potential-energy surface. Contours are in increments of 0.25 eV starting at 0.25 eV. Superimposed on the neutral surface (thin lines) is a projection of the  $\Psi_{00}$  (thick gray lines) and  $\Psi_{10}$  (thick dark lines) anion vibrational wave functions. These contours are every 20% showing a total of 90%. This projection identifies the Franck-Condon region on the neutral surface following the photodetachment of an electron on the anion. The Franck-Condon region lies in the entrance channel to the  $\text{OH} + \text{NH}_3 \rightarrow \text{H}_2\text{O} + \text{NH}_2$  reaction.

pointing towards the N atom, however, a minimum is only found when the symmetry is relaxed to  $C_1$ . This is due to the Jahn-Teller effect that breaks the symmetry of the molecule. Frequency calculations confirm this result; if the complex is restricted to  $C_{3v}$  or  $C_s$  symmetry, there is at least one negative eigenvalue. Similar to the reactant complex, the transition state of the neutral was also found to have  $C_1$  symmetry. The product complex, on the other hand, has  $C_s$  symmetry.

Like the anion surface, the neutral potential-energy surface was generated by calculating the energy at many different  $r_{\text{OH}}$  and  $r_{\text{NO}}$  values with all other parameters constant. The distance  $r_{\text{OH}}$  was scanned from 0.8 to 3 Å and  $r_{\text{NO}}$  from 1.5 to 5 Å in 0.1 Å increments. This surface is displayed in Fig. 6 (thin lines). There are two distinct minima, one in the entrance channel and one in the exit channel to the  $\text{OH} + \text{NH}_3 \rightarrow \text{H}_2\text{O} + \text{NH}_2$  reaction. The locations of these

TABLE II. Relative energies and full widths at half maximum (FWHM) for the origin peaks in the  $\text{OH}^-(\text{NH}_3)_n$ ,  $n=0-2$  photoelectron spectra.

| Peak                         | Relative energy (eV) | FWHM (meV) |
|------------------------------|----------------------|------------|
| $\text{OH}^-$                |                      |            |
| <i>a</i>                     | 0                    | 30         |
| $\text{OH}^-(\text{NH}_3)$   |                      |            |
| <i>A</i>                     | 0.75                 | 170        |
| $\text{OH}^-(\text{NH}_3)_2$ |                      |            |
| <i>A''</i>                   | 1.22                 | 245        |

minima agree with those found in the stationary points calculations.

The Franck-Condon region for the photodetachment process has been located by projecting the anion vibrational wave functions onto the neutral surface. Also shown in Fig. 6, are the projections of 90% of the  $\Psi_{00}$  (thick gray lines) and  $\Psi_{10}$  (thick dark lines) wave functions. The Franck-Condon region lies in the entrance channel to the  $\text{OH} + \text{NH}_3 \rightarrow \text{H}_2\text{O} + \text{NH}_2$  reaction. As illustrated, the wave functions span over 0.5 eV along both coordinates. It is possible to access a large range of energies including high on the repulsive wall and extending towards the transition state on the neutral potential-energy surface.

## IV. DISCUSSION

### A. Assignments

As discussed earlier, the  $\text{OH}^-(\text{NH}_3)$  and  $\text{OH}^-(\text{NH}_3)_2$  spectra are dominated by a single peak (*A*, *A''*, respectively) similar to that seen in the  $\text{OH}^-$  spectrum (peak *a* in Fig. 3). This suggests that the  $\text{OH}^-$  is solvated by the  $\text{NH}_3$  molecules and that the negative charge remains localized on the OH chromophore. The main peaks in the  $n=1,2$  spectra arise from the photodetachment of an electron from the solvated  $\text{OH}^-$  chromophore within the clusters.

The FWHM of peak *a* is  $\sim 30$  meV, considerably larger than the energy resolution of the spectrometer, due to unresolved rotational structure. There is a further increase in the width of the origin peak (*A*, *A''* in Fig. 3) that we attribute to the activation of many low-frequency van der Waals vibrations following photodetachment. There is also a noticeable shift in energy of the origin upon the addition of  $\text{NH}_3$  solvent. The  $n=1$  spectrum is shifted 0.75 eV to higher energy of the  $\text{OH}^-$  peak<sup>22-24</sup> and the  $n=2$  spectrum is an additional 0.47 eV higher. The relative energies and widths of the origin peaks are listed in Table II. This shift to higher energy is consistent with a stabilization of the anion with respect to the neutral upon solvation. These results are similar to what was reported for  $\text{OH}^-(\text{N}_2\text{O})_n$ ,  $\text{H}^-(\text{NH}_3)_n$ , and  $\text{NH}^-(\text{NH}_3)_n$  where the spectra are all dominated by a single peak that resembles that observed in the  $\text{OH}^-$ ,  $\text{H}^-$ , and  $\text{NH}^-$  photoelectron spectra.<sup>15-17</sup>

The absence of a shift for peak *A'* in the deuterated spectrum (see Fig. 2) confirms the assignment of peak *A* as the origin in the  $\text{OH}^-(\text{NH}_3)$  spectrum. On the other hand, peak *B'* shifts to lower electron binding. Specifically, the frequency decreases from 2825 to 2340  $\text{cm}^{-1}$  upon deute-

rium substitution, characteristic of a vibrational motion that involves the H(D) atom. Such a high frequency can only be attributed to the O–H or the N–H stretching modes. However, only the later is expected to show some Franck–Condon progression of peaks due to the larger change in geometry of this bond upon detachment. Thus, peak  $B(B')$  is assigned as one quantum of vibration in the N–H2(D2) stretching motion. Although the frequency of an N–H stretch in bare ammonia is  $3417\text{ cm}^{-1}$ , Neumark and co-workers have shown that hydrogen motions within reactive complexes, far from the dissociation asymptote and near the transition state, are shifted to lower energy.<sup>11,13</sup> Similarly, in the photoelectron spectra of  $\text{D}^-(\text{ND}_3)_n$ , and  $\text{ND}^-(\text{ND}_3)_n$ , Bowen and co-workers found that the vibrational frequency between the origin and the peaks to higher electron binding energy decreased in the deuterated spectra relative to that measured in the hydrogen containing clusters.<sup>16,17</sup> For these systems, the peaks were assigned as stretching modes within the  $\text{NH}_3(\text{ND}_3)$ .

## B. Energetics

The geometry of the  $\text{OH}^-(\text{NH}_3)$  anion complex is different than that of the minimum on the neutral surface corresponding to the  $\text{OH}(\text{NH}_3)$  reactant complex, as illustrated in Figs. 4(a) and 4(b), primarily a result of internal rotation of the OH constituent. As a consequence, many low-frequency modes are activated following electron detachment, and these low-frequency modes are not resolved in the experiment, making an accurate, purely experimental determination of the  $\text{EA}[\text{OH}(\text{NH}_3)]$  very difficult. In this case, however, this quantity can be estimated utilizing a combination of results from experiments and *ab initio* calculations, employing a thermochemical cycle,

$$\text{EA}[\text{OH}(\text{NH}_3)] = \text{EA}[\text{OH}] + D_0[\text{OH}^-(\text{NH}_3)] - D_0[\text{OH}(\text{NH}_3)].$$

The first term is known is the largest and is very accurately known experimentally<sup>22–24</sup> to be  $1.828\,664\text{ eV}$ . The ionic dissociation energy is smaller and can be relatively accurately calculated to be  $0.65\text{ eV}$ , including zero-point corrections. The neutral bond energy is much smaller and much more difficult to calculate accurately, but is around  $0.15\text{ eV}$ , again with zero-point corrections included. The calculated value of  $0.15\text{ eV}$  for  $D_0[\text{OH}(\text{NH}_3)]$  is a bit higher than other experimentally determined values for the binding energies of  $\text{X}-\text{NH}_3$  ( $\text{X}=\text{HCCH}, \text{HCN}, \text{CO}_2, \text{NH}_3, \text{Ar}, \text{N}_2\text{O},$  and  $\text{OCS}$ ) complexes; all of these values are  $\leq 0.12\text{ eV}$ .<sup>25</sup> Using  $0.12\text{ eV}$  for  $D_0[\text{OH}(\text{NH}_3)]$  results in the  $\text{EA}=2.36\text{ eV}$ . Thus we estimate  $\text{EA}[\text{OH}(\text{NH}_3)]=2.35\pm 0.07\text{ eV}$ ; the error bar comes from our experience with errors found for experimentally checked ionic dissociation energies calculated for similar systems. All of the energetics for this system are collected and summarized in the diagram shown in Fig. 7. All calculated values include the zero point energy corrections; accurate experimental values (shown in bold face) are used if known. Extrapolation of the  $\text{OH}^-(\text{NH}_3)$  spectrum to  $0\text{ K}$  shows nonzero intensity in the electron binding energy range of the calculated  $\text{EA}[\text{OH}(\text{NH}_3)]$  ( $2.28\text{--}2.42\text{ eV}$ , including

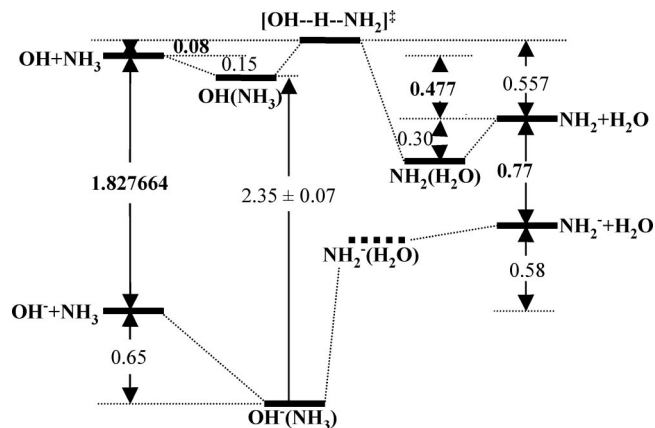


FIG. 7. A schematic of the energetics associated with the stationary points along the anion and neutral surfaces. All values are in electron volts and have been determined using second-order Møller–Plesset perturbation theory including all electrons and the  $6\text{-}31+\text{G}^{**}$  basis set. Values in bold have been determined experimentally. Using the calculated values for the binding energy of  $\text{OH}^-(\text{NH}_3)$  and  $\text{OH}(\text{NH}_3)$  and the experimental value for the electron affinity (EA) of OH, an estimate of the EA for  $\text{OH}(\text{NH}_3)$  is  $2.35\pm 0.05\text{ eV}$ .

error bars), suggesting that the  $0\text{--}0$  transition has detectable intensity, although the actual origin can not be identified based on our data alone.

As shown in Fig. 7, the energy difference between the TS and the neutral reactant complex is  $0.23\text{ eV}$ . If the adiabatic electron affinity is  $2.35\text{ eV}$ , the energy at the transition state is  $2.58\text{ eV}$ . This is at the region of maximum intensity of the main peak A (width  $170\text{ meV}$ ) in the photoelectron spectrum. This result provides very strong evidence that the transition state is energetically accessible following electron photodetachment. The second peak in the spectrum extends almost  $1\text{ eV}$  and involves the N–H2 stretching motion, which is along the reaction coordinates. In addition, the low energy  $\Psi_{10}$  anion wave function provides excitation in a mode leading almost directly to the transition state, again suggesting not only that photodetachment leaves the neutral with sufficient internal energy to reach the transition state, but also that much of this energy is deposited in modes leading directly toward the transition state.

It is important to point out that the potential-energy surface in Fig. 6 is based purely on calculations. Although the overall shape of the potential-energy surface is correct, the calculations predict (as expected at this level of calculation) that the barrier height is much larger ( $0.42\text{ eV}$ ) than that determined experimentally ( $0.08\text{ eV}$ ) and, therefore, the barrier in Fig. 6 is much higher than that discussed above. It is still possible, however, to see that the transition state is accessible. If a higher basis set is used in calculating the energetics, the barrier height will go down and it would be more obvious that the wave functions could spread across the transition state region.

The *ab initio* geometry optimization calculations suggest that the  $\text{OH}+\text{NH}_3\rightarrow\text{NH}_2+\text{H}_2\text{O}$  reaction has an early transition state. This is evident by comparing the distances of the bonds that are formed (O–H2) and broken (N–H2) during reaction within the transition state to those in the reactant and product minimum energy structures. The N–H2 bond

that is broken increases by  $\sim 10\%$  from reactants to the transition state. It is difficult to characterize the O–H bond that is formed since there is a large geometry change between the reactants and transition state. In order to proceed from the reactants to the transition state, there needs to be a significant internal rotation of the OH species with respect to the  $\text{NH}_3$  so that the O atom can bind to one of the H atoms on the nitrogen.

### C. Comparisons with other studies

There have been several studies that were successful in probing the transition states of neutral reactions. Neumark, Lineberger, and co-workers were able to access the transition state of the  $\text{OH} + \text{H}_2 \rightarrow \text{H} + \text{H}_2\text{O}$  reaction by photodetaching an electron from the  $\text{H}_3\text{O}^-$  anion.<sup>14</sup> They saw a similar effect in the spectrum upon deuterium substitution as seen in the present work, however, the results of the polarization and temperature studies were different. The photoelectron spectra of  $\text{H}_3\text{O}^-$  and  $\text{D}_3\text{C}^-$  revealed a strong dependence on the laser polarization and vibrational temperature. It was clear that the peaks in the spectra resulted from different electronic transitions. The difference in the spectra obtained at  $\theta = 0^\circ$  and  $90^\circ$  and under room temperature and liquid nitrogen cooled conditions result from the formation of both forms of anion clusters,  $\text{OH}^-(\text{H}_2)$  and  $\text{H}^-(\text{H}_2\text{O})$ , in the flow tube. Photodetachment of an electron from these clusters accessed both the reactant and product sides of the neutral potential-energy surface. *Ab initio* calculations concluded that the anion potential-energy surface contained two minima corresponding to  $\text{OH}^-(\text{H}_2)$  and  $\text{H}^-(\text{H}_2\text{O})$ . This is in contrast to the present experiment where only one minimum is predicted on the anion surface. The reaction dynamics occurring on other neutral potential-energy surfaces have been characterized in a similar manner. Transition state spectroscopy has been implemented on the  $\text{I} + \text{HI}$ ,  $\text{Br} + \text{HI}$ , and  $\text{H} + \text{F}_2$  reactions, to name a few.<sup>11</sup>

There have been multiple studies on the neutral  $\text{OH} + \text{NH}_3 \rightarrow \text{NH}_2 + \text{H}_2\text{O}$  reaction, many of which include the determination of the barrier height. Luch and co-workers<sup>5</sup> performed *ab initio* calculations on the  $\text{OH} + \text{NH}_3$  reaction using  $\text{MP2}/6\text{-}31\text{G}^{**}$ . These calculations determined the geometry of the transition state structure and an IRC was also constructed. The geometry of the TS agrees very well with that displayed in Fig. 4(c). In addition, a barrier of 5.1 kcal/mole is reported. More recently, a reaction-path dynamics calculation yielded a barrier height of 3.65 kcal/mole.<sup>9</sup>

*Ab initio* calculations by Espinosa–Garcia and co-workers<sup>6</sup> also determined minimum energy configurations for the reactant, product, and transition state complexes along the reaction coordinate as well as the corresponding harmonic vibrational frequencies using the same method and basis set as Luch and co-workers but with full electron correlation,  $\text{MP2}(\text{FULL})/6\text{-}31\text{G}^{**}$ . After determining the transition state, an IRC calculation also was performed. These results also indicated that there is an early transition state to reaction. With additional calculations, they concluded that the reactant complex was unstable after taking the zero-point energy into consideration; there were no bound vibrational levels in the potential. Their structure was extremely differ-

ent from the one determined in our calculations which could be the explanation for the instability. The  $C_s$  geometry that they reported was not found to be a minimum in our calculations with the addition of the diffuse functions. It is important to note that the addition of the diffuse functions in our calculations was necessary for the calculation of the anion geometries and frequencies. For comparison purposes, the same basis set was used for the neutral complexes. These calculations by Espinosa–Garcia and co-workers determined a barrier height to reaction of 3.5 kcal/mole.

There have been many experimental studies, using a various number of methods, which have determined the rate of the  $\text{OH} + \text{NH}_3 \rightarrow \text{NH}_2 + \text{H}_2\text{O}$  reaction.<sup>1–4</sup> The most recent, by Y.-P. Lee and co-workers, utilized flash photolysis and laser-induced fluorescence to do their kinetic studies.<sup>4</sup> A fit of the rate coefficients to the Arrhenius equation yields an activation barrier of  $\sim 1.85$  kcal/mole. This value is a good representation of the other experimental values available in the literature but much lower than calculated values. All of the above values for the barrier height to reaction are much smaller than the 8 kcal/mole obtained in our *ab initio* calculations.

### V. CONCLUSIONS

The negative ion photoelectron spectra of  $\text{OH}^-(\text{NH}_3)$ ,  $\text{OH}^-(\text{NH}_3)_2$ , and  $\text{OD}^-(\text{ND}_3)$  have been recorded. The  $\text{OH}^-(\text{NH}_3)$  and  $\text{OD}^-(\text{ND}_3)$  spectra consist of a dominant peak (A) with a less intense peak (B) to higher electron binding energy. By using both experimental and theoretical results, peak A has been assigned as the origin and peak B to a vibrationally excited N–H mode within the cluster. The spectra have been compared to the  $\text{OH}^-$  photoelectron spectrum and we conclude that the negative charge remains largely localized on the  $\text{OH}^-$  chromophore after solvation by the  $\text{NH}_3$  molecules. Since vibrational structure is unresolved in the spectrum and the geometries of the anion and neutral are significantly different, an accurate purely experimental determination of the EA could not be extracted.

*Ab initio* calculations on the anion and neutral surfaces have been carried out using  $\text{MP2}(\text{FULL})/6\text{-}31 + \text{G}^{**}$  to aid in the analysis of the spectra. The stationary points along the anion and neutral surfaces have been found through geometry optimizations and frequency calculations; partial potential-energy surfaces have been generated. We find only one minimum on the anion surface, corresponding to the  $\text{OH}^-(\text{NH}_3)$  complex while two minima,  $\text{OH}(\text{NH}_3)$  and  $\text{H}_2\text{O}(\text{NH}_2)$ , and a transition state were found on the neutral surface. An estimate of  $\text{EA}[\text{OH}(\text{NH}_3)] = 2.35 \pm 0.07$  eV was obtained using calculated dissociation energies and the experimental  $\text{EA}(\text{OH})$  in a thermochemical cycle; this result shows conclusively that electron photodetachment accesses the ground state of the complex with at least modest intensity. The width of the first broad peak in the spectrum also indicates that sufficient energy is deposited in the neutral complex to surmount the barrier to reaction.

The  $\Psi_{00}$  and  $\Psi_{10}$  anion vibrational wave functions have been calculated. These wave functions were projected onto the neutral surface in order to determine the region of the neutral surface that is accessed following the electron detach-

ment. These calculations show that the transition state for OH+NH<sub>3</sub>→NH<sub>2</sub>+H<sub>2</sub>O reaction is near the region of maximum intensity in the spectrum, and that the nature of the excitation following electron detachment is such that it may not be directly probed, however, there is enough energy remaining in the system to surmount the activation barrier to reaction. As a consequence, this complex should be an ideal candidate for ultrafast time domain studies using a negative ion-neutral-positive ion charge reversal approach.<sup>26</sup>

## ACKNOWLEDGMENT

This work is funded by the National Science Foundation.

- <sup>1</sup>R. A. Perry, R. Atkinson, and J. N. Pitts, Jr., *J. Chem. Phys.* **64**, 3237 (1976).
- <sup>2</sup>J. A. Silver and C. E. Kolb, *Chem. Phys. Lett.* **75**, 191 (1980).
- <sup>3</sup>R. D. Stephens, *J. Phys. Chem.* **88**, 3308 (1984).
- <sup>4</sup>E. Wei-Guang Diau, T.-L. Tso, and Y.-P. Lee, *J. Phys. Chem.* **94**, 5261 (1990).
- <sup>5</sup>X. Gimenez, M. Moreno, and J. M. Lluch, *Chem. Phys.* **165**, 41 (1992).
- <sup>6</sup>J. C. Corchado, F. J. Olivares, and J. Espinosa-Garcia, *J. Phys. Chem.* **97**, 9129 (1993).
- <sup>7</sup>J. Espinosa-Garcia and J. C. Corchado, *J. Chem. Phys.* **101**, 8700 (1994).
- <sup>8</sup>G. Leroy, M. Sana, and A. Tinant, *Can. J. Chem.* **63**, 1447 (1985).
- <sup>9</sup>J. C. Corchado, J. Espinosa-Garcia, W.-P. Hu, I. Rossi, and D. G. Truhlar, *J. Phys. Chem.* **99**, 687 (1995).
- <sup>10</sup>G. Nyman, *J. Chem. Phys.* **104**, 6154 (1996).
- <sup>11</sup>S. E. Bradforth, A. Weaver, D. W. Arnold, R. B. Metz, and D. M. Neumark, *J. Chem. Phys.* **92**, 7205 (1990).
- <sup>12</sup>S. E. Bradforth, D. W. Arnold, R. B. Metz, A. Weaver, and D. M. Neumark, *J. Phys. Chem.* **95**, 8066 (1991).
- <sup>13</sup>D. M. Neumark, *Acc. Chem. Res.* **26**, 33 (1993).
- <sup>14</sup>E. de Beer, E. H. Kim, D. M. Neumark, R. F. Gunion, and W. C. Lineberger, *J. Phys. Chem.* **99**, 13627 (1995).
- <sup>15</sup>J. B. Kim, P. G. Wenthold, and W. C. Lineberger, *J. Chem. Phys.* **108**, 830 (1998).
- <sup>16</sup>J. T. Snodgrass, J. V. Coe, C. B. Freidhoff, K. M. McHugh, and K. H. Bowen, *Faraday Discuss. Chem. Soc.* **86**, 241 (1988).
- <sup>17</sup>J. T. Snodgrass, J. V. Coe, C. B. Freidhoff, K. M. McHugh, S. T. Arnold, and K. H. Bowen, *J. Phys. Chem.* **99**, 9675 (1995).
- <sup>18</sup>K. M. Ervin and W. C. Lineberger, in *Advances in Gas Phase Ion Chemistry*, Vol. 1, edited by N. G. Adams and L. M. Babcock (JAI, Greenwich, 1992), p. 121.
- <sup>19</sup>J. Cooper and R. N. Zare, *J. Chem. Phys.* **48**, 942 (1968).
- <sup>20</sup>GAUSSIAN 94, M. J. Frisch, G. W. Trucks, H. B. Schlegel, P. M. W. Gill, B. G. Johnson, M. A. Robb, J. R. Cheeseman, T. Kieth, G. A. Petersson, J. A. Montgomery, K. Raghavachari, M. A. Al-Laham, V. G. Zakrewski, J. V. Ortiz, J. B. Foresman, J. Cioslowski, B. B. Stefanov, A. Nanayakkara, M. Challacombe, C. Y. Peng, P. Y. Ayala, W. Chen, M. W. Wong, J. L. Andres, E. S. Replogle, R. Gomperts, R. L. Martin, D. J. Fox, J. S. Binkley, D. J. Defrees, J. Baker, J. P. Stewart, M. Head-Gordon, C. Gonzalez, and J. A. Pople (Gaussian Inc., Pittsburgh, PA, 1995).
- <sup>21</sup>D. C. Harris and M. D. Bertolucci, *Symmetry and Spectroscopy* (Dover, New York, 1978).
- <sup>22</sup>H. Hotop, T. A. Patterson, and W. C. Lineberger, *J. Chem. Phys.* **60**, 1806 (1974).
- <sup>23</sup>P. A. Schulz, R. D. Mead, P. L. Jones, and W. C. Lineberger, *J. Chem. Phys.* **77**, 1153 (1982).
- <sup>24</sup>J. R. Smith, J. B. Kim, and W. C. Lineberger, *Phys. Rev. A* **55**, 2036 (1997).
- <sup>25</sup>G. T. Fraser, D. D. Nelson, Jr., A. Charo, and W. Klemperer, *J. Chem. Phys.* **82**, 2535 (1985).
- <sup>26</sup>D. W. Boo, Y. Ozaki, L. H. Andersen, and W. C. Lineberger, *J. Phys. Chem. A* **101**, 6688 (1997).